Journal of Structural Geology, Vol. 13, No. 4, pp. 459 to 469, 1991
Printed in Great Britain

0191-8141/91 $03.00+0.00

Experiments on faulting in a two-layer cover sequence overlying a reactivated basement fault with oblique-slip

P. RICHARD

Laboratoire de Tectonophysique, Université de Rennes I, Avenue du général Leclerc, 35042 Rennes Cédex, France

(*Received* 20 *October* 1989; *accepted in revised form* 7 *October* 1990)

Abstract—Two series of experiments were undertaken to investigate the development of faults in a cover sequence overlying a reactivated basement fault with oblique-slip. The experiments represent physical models properly scaled to account for gravitational forces, brittle behaviour of the upper cover and ductile behaviour of evaporites in the lower cover. Models were made with a Coulomb layer (sand) overlying a Newtonian ductile layer (silicone putty). In each series, the thickness of the silicone layer was varied from each experiment to the next. In all normal-wrench experiments, a domain of faults appeared in the brittle layer. Vertical offsets were mostly of normal sense, but some reverse faults occurred in experiments with thick silicone layers. The thicker the silicone, the wider the fault domain. The deformation zone was, in all cases, limited to the faulted domain. In the reverse-wrench experiments, discrete reverse Riedel faults appeared without a silicone layer. As the silicone layer became thicker, the importance of the reverse faults diminished. With the thickest layer of silicone (3 cm), no faults appeared in the overburden, but a monoclinal flexure accommodated the dip-slip component. In the presence of silicone, the deformation zone was not limited to a faulted domain, and the strike-slip component was accommodated by a bulk shearing of the overburden in the uplifted compartment. These experiments demonstrate that, in basins deformed in oblique-slip mode, any deformation that is localized along discrete faults at the basement level becomes distributed over a much wider zone of overburden when this overlies an interval of evaporites.

INTRODUCTION

IN MANY areas, sedimentary cover overlies a faulted basement. In such cases, deformation in the brittle cover is strongly dependent on the localization of deformation on the basement faults. When an interval of evaporites or clay lies between the cover and the basement, the deformation in the cover is often geometrically independent from the deformation accommodated in the basement (Fig. 1). This structural influence of evaporites or clay is caused mainly by its contrast in flow. In the present experimental study, we have modelled the influence of an interval of evaporites on the deformation of a brittle cover overlying a basement fault reactivated in oblique (reverse-wrench or normal-wrench) mode.

EXPERIMENTS

Previous work

Many experimental studies (Cloos 1928, Riedel 1929, Wilcox *et al.* 1973) have simulated the deformation of a sedimentary cover above a reactivated single basement fault in strike-slip mode, by placing a cake of unbroken clay on two basal rigid plates which could be moved parallel to one another. Sand has also been used for wrench faulting experiments (Naylor *et al.* 1986, Richard & Cobbold 1989). The clay and sand were used to model the brittle behaviour of natural rocks. To model the behaviour of ductile natural rocks, silicone putty has been used (Davy 1986, Vendeville *et al.* 1986). The formation of positive flower structures at various scales has been investigated in experiments in which a pack of sand overlying a silicone layer was deformed in a convergent wrench context (Richard & Cobbold 1989, Richard 1990). Simultaneous folding and faulting of a multilayered ductile–brittle cover in strike-slip mode has been performed by deforming multilayered silicone–sand models (Richard 1990, Richard *et al.* in press). With this present work, the influence of a viscous layer on the faulting of a sedimentary cover in oblique-slip mode has been investigated.

Scaling of brittle–ductile experiments

The theory of scale models has been applied to the earth sciences by Hubbert (1937) and Ramberg (1967). An analogue model is representative of a natural example if the experimental and natural systems are dynamically similar; this requires both (1) similar distributions of stresses and forces and (2) similar rheologies and densities.

If inertial forces are negligible, the balance of forces is expressed as

$$\partial \boldsymbol{\sigma}_{ij} / \partial \mathbf{X}_j + \rho \mathbf{g}_i = 0, \quad (1)$$

where $\boldsymbol{\sigma}_{ij}$ are stresses, $\mathbf{X}_j$ are length vectors, $\mathbf{g}_i$ are components of the gravity vector and ρ is density. In equation (1) we use Cartesian vector and tensor components, with the summation convention for repeated suffixes. To compare an experimental and a natural system which have different geometrical and temporal

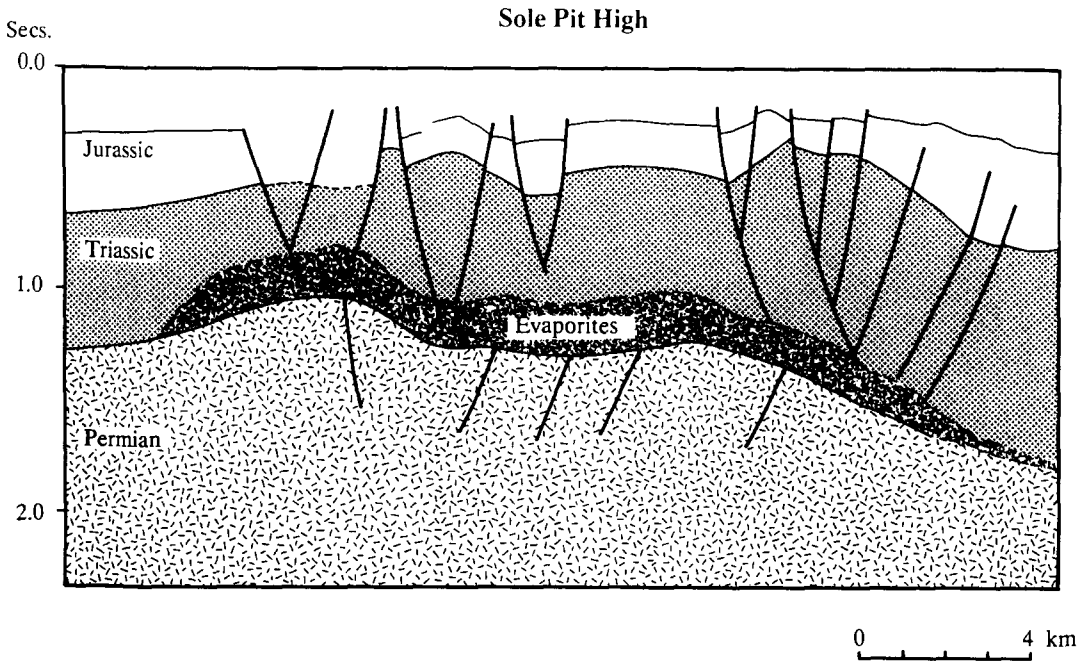

Fig. 1. Interpretation of a seismic line across the Sole Pit High (North Sea). A detachment zone (Lower Triassic evaporites) separates cover and basement fault systems (redrawn from Van Hoorn 1987).

scales, it is convenient to consider scale ratios, between an experimental parameter (force, stress, length, etc.) and its natural counterpart. Various scale ratios have been defined (subscript m and n refer to model and nature, respectively):

$$\begin{aligned} \text{length ratio} &= L^* = L_m/L_n \\ \text{stress ratio} &= \sigma^* = \sigma_m/\sigma_n \\ \text{gravity ratio} &= g^* = g_m/g_n \\ \text{density ratio} &= \rho^* = \rho_m/\rho_n \\ \text{viscosity ratio} &= \mu^* = \mu_m/\mu_n. \end{aligned} \tag{2}$$

Equation (1) applied to the model can be written using the parameters of the natural system and the scale ratios:

$$\sigma^*(L^*)^{-1}(\boldsymbol{\sigma}_{ijn}/\mathbf{X}_{jn}) + \rho^* \cdot \mathbf{g}_i^* \cdot (\rho_n \cdot \mathbf{g}_{in}) = 0. \tag{3}$$

To be verified in nature, this equation requires that

$$\sigma^* = L^* \cdot \rho^* \cdot g^*. \tag{4}$$

All the experiments were done in the Earth's field of gravity and thus $g^* = 1$. The difference in density between analogue materials and natural rocks is negligible and thus we consider $\rho^* = 1$. Equation (4) reduces to

$$\sigma^* = L^*. \tag{5}$$

For a brittle material with a Mohr–Coulomb criterion of failure,

$$\tau = C + \sigma_n \tan \Phi, \tag{6}$$

where τ and σ_n are, respectively, the shear stress and the normal stress acting on the failure surface. Φ is the angle of internal friction of the material and C is the cohesion with dimensions of stress. This equation expresses a time-independent rheological behaviour.

In the upper brittle crust (5–10 km) rocks apparently have an angle of internal friction close to 30°, and a cohesion that is negligible compared with values of mean stress in the crust (Byerlee 1978, Vendeville 1987). The sand used in the experiments is a dry quartz sand with negligible cohesion and an angle of internal friction Φ = 30–32°. Thus both the natural example and the model satisfy equation (6) and the sand is correctly scaled for the brittle behaviour of the upper crust.

A Newtonian ductile material has rheological behaviour according to the equation

$$\sigma'_{ij} = \mu \cdot \dot{\varepsilon}_{ij}, \tag{7}$$

where μ is viscosity, $\dot{\varepsilon}$ is strain-rate and σ' is deviatoric stress.

Using the scale ratios (2) and the equations (6) and (4) yields

$$\sigma^* = \mu^* \cdot \dot{\varepsilon}^* = L^*. \tag{8}$$

Instead of using the ratio of strain-rates, $\dot{\varepsilon}^*$, we can use the ratio of boundary velocities (displacement rates), U^*, and write

$$\dot{\varepsilon}^* = U^*/L^*. \tag{9}$$

Substituting (9) in (8), we obtain

$$\mu^* \cdot U^* = (L^*)^2. \tag{10}$$

Equation (10) can be written

$$\mu_m/\mu_n \cdot U_m/U_n = (L_m/L_n)^2 \tag{11}$$

with μ in Pa s, U in m s^{-1} and L in m.

Figure 2 shows the predicted natural rock viscosity, μ_n, calculated according to equation (11), for silicone viscosity of 2×10^4 Pa s and for various fixed values of L^*, U_m and U_n. For reasonable ranges of the latter

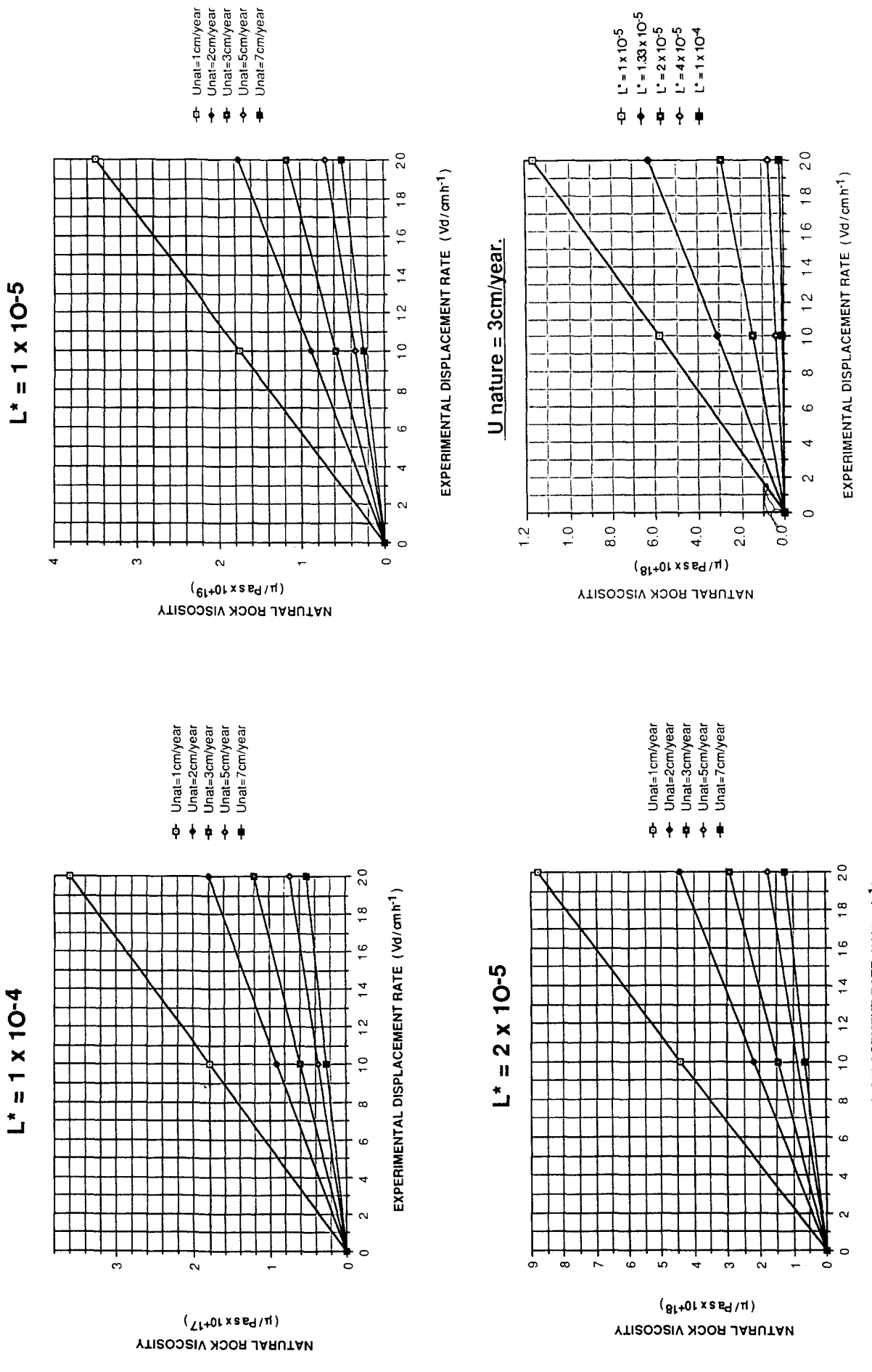

Fig. 2. Influence of the experimental displacement rate on the natural rock viscosity with different length ratios ($L^* = L_m/L_n$) and natural displacement rate (U_n).

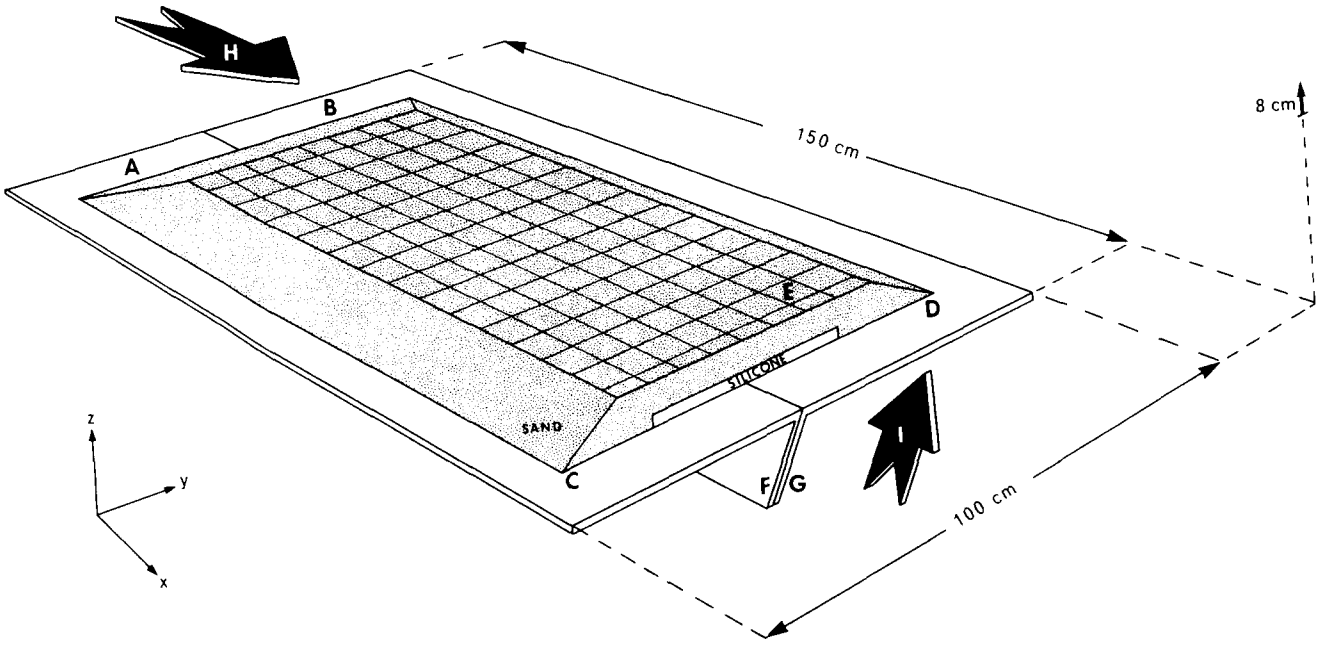

Fig. 3. Block diagram of the experimental apparatus. A and B—Basal plates (150 × 50 cm each); C and D—Characteristic section of an undeformed sand–silicone model; E—Grid of passive markers on the free surface of the model; F and G—Variable attitude flaps; H and I—Imposed displacements to plate B. During the deformation, a velocity discontinuity is created beneath the middle plane of the model.

parameter, μ_n ranges from 10^{17} to 10^{19} Pa s. This is consistent with the evaporite viscosities estimated by Odé (1968).

Experimental apparatus

The experimental apparatus used for the oblique-slip experiments consisted of a large table (2 × 1.5 m) divided into two halves. The central part of the apparatus is represented in Fig. 3. One half (B) can be moved simultaneously laterally (H) and vertically (I) past the other (A), which is fixed, by two geared motor drives, thus modelling oblique-slip motions on a single basement fault. The dip of the basement fault can be changed by varying the attitude of two flaps (F, G), and thus, reverse or normal motions on the basement fault can be obtained. Different ratios of strike-slip/dip-slip motions (*SS/DS*) are fixed by changing the respective speed of the two geared motor drives. Each *SS/DS* ratio corresponds to a particular oblique-slip motion (*OS*), and to a particular angle, with the relation $SS/DS = \tan \alpha$, where α is the pitch of the slip vector upon the fault plane.

Model materials

Experiments were made using two different materials: a sand (100% quartz) and a silicone putty (gomme GS1R, manufactured by Rhône-Poulenc, France). The sand is a Coulomb material, with an angle of internal friction Φ = 30–32°, similar to the angle of internal friction determined experimentally for rocks under low pressures and temperatures (Byerlee 1978). The deformation of the sand is time-independent. The sand is appropriate for modelling the brittle behaviour of upper crustal rocks at basin scale (Horsfield 1977, Vendeville 1987). The silicone putty has an almost perfectly Newtonian ductile behaviour, a viscosity of 2×10^4 Pa s, and a density of 1.15. These properties make the silicone a good analogue for ductile evaporites at the basin scale (Vendeville *et al.* 1986, Vendeville 1987).

Models were scaled using the equations previously discussed. Scale ratios between models and natural examples are, respectively, 2×10^{-5} for length (10^{-2} m represents 500 m), 1.3×10^{-14} for viscosities (implying a viscosity of 1.5×10^{18} Pa s for evaporites) and 7×10^{-10} for time (1 h of experiment represents 170,000 years). A length ratio (L^*) of 2×10^{-5} (10^{-2} m represents 500 m) has been chosen. For a fixed natural displacement rate of 3 cm yr^{-1} (9.5×10^{-10} m s^{-1}), an experimental displacement rate in the range 5–20 cm h^{-1} (1.4×10^{-5}–5.6×10^{-5} m s^{-1}, can then be used without influence on the natural rock viscosity (Fig. 2), which ranges between 1×10^{18} and 3×10^{18} Pa s. These values are consistent with the evaporite viscosities (Odé 1968).

Experimental procedure

Reverse or normal oblique-slip faulting were each studied in a series of four experiments. The total thickness of each model was 8 cm. The horizontal dimensions were about 70–80 cm (length) by 50–60 cm (width). In each series, four types of models were used: type 1, an 8 cm thick layer of sand; type 2, a 7 cm thick layer of sand overlying a 1 cm thick layer of silicone; type 3, 6 cm of sand overlying 2 cm of silicone; type 4, 5 cm of sand overlying 3 cm of silicone. The strike-slip/dip-slip ratio was the same for each experiment (*SS/DS* = 1). The oblique-slip has been fixed, in each experiment, at 4 cm. In normal oblique-slip experiments, the dip of the base-

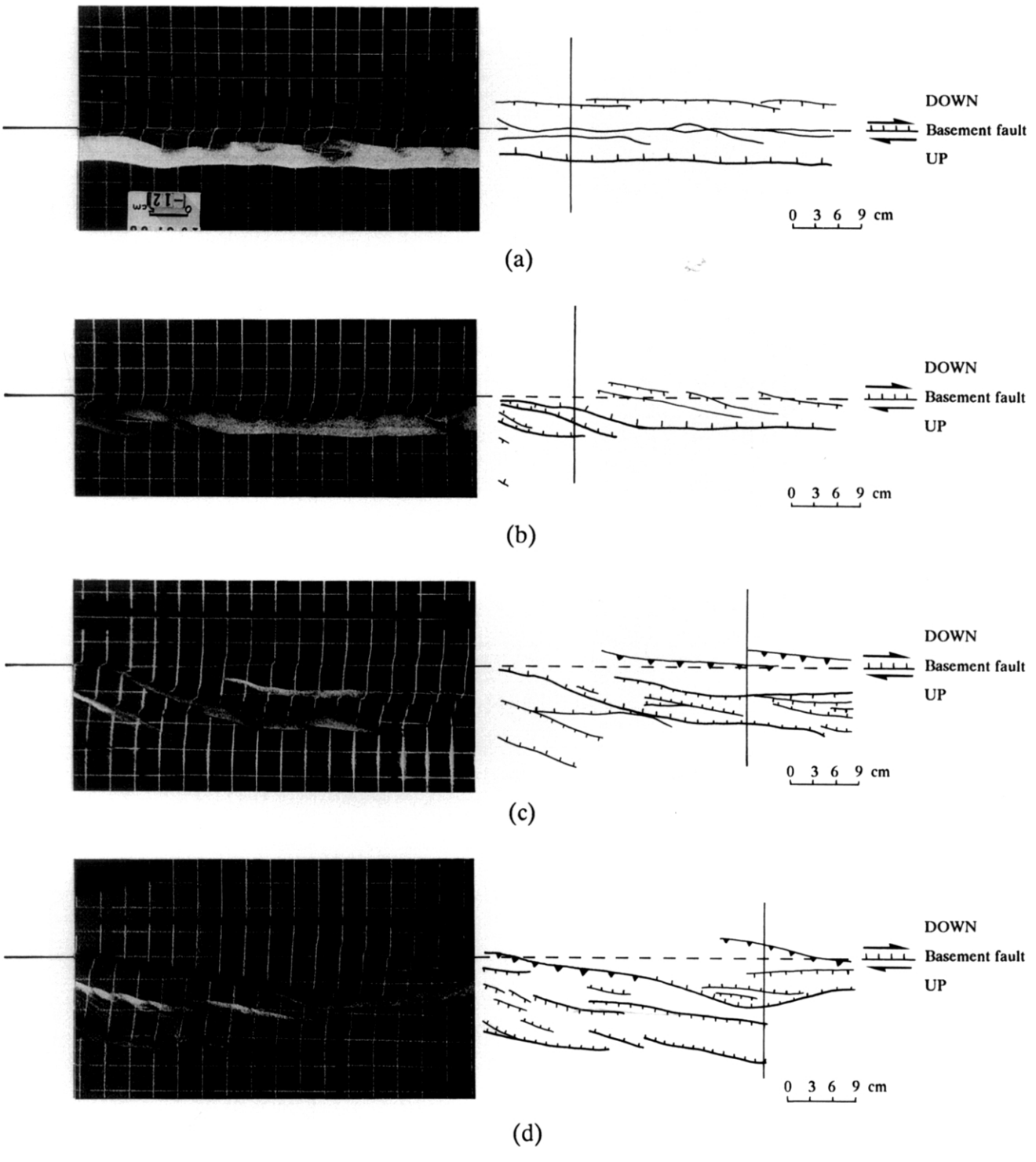

Fig. 4. Normal oblique-slip experiments ($SS/DS = 1$). Photographs and line drawings of faults developed with the same normal oblique-slip (4 cm), above a 45° basement fault, with an underlying 0, 1, 2 and 3 cm thick (a–d) layer of silicone.

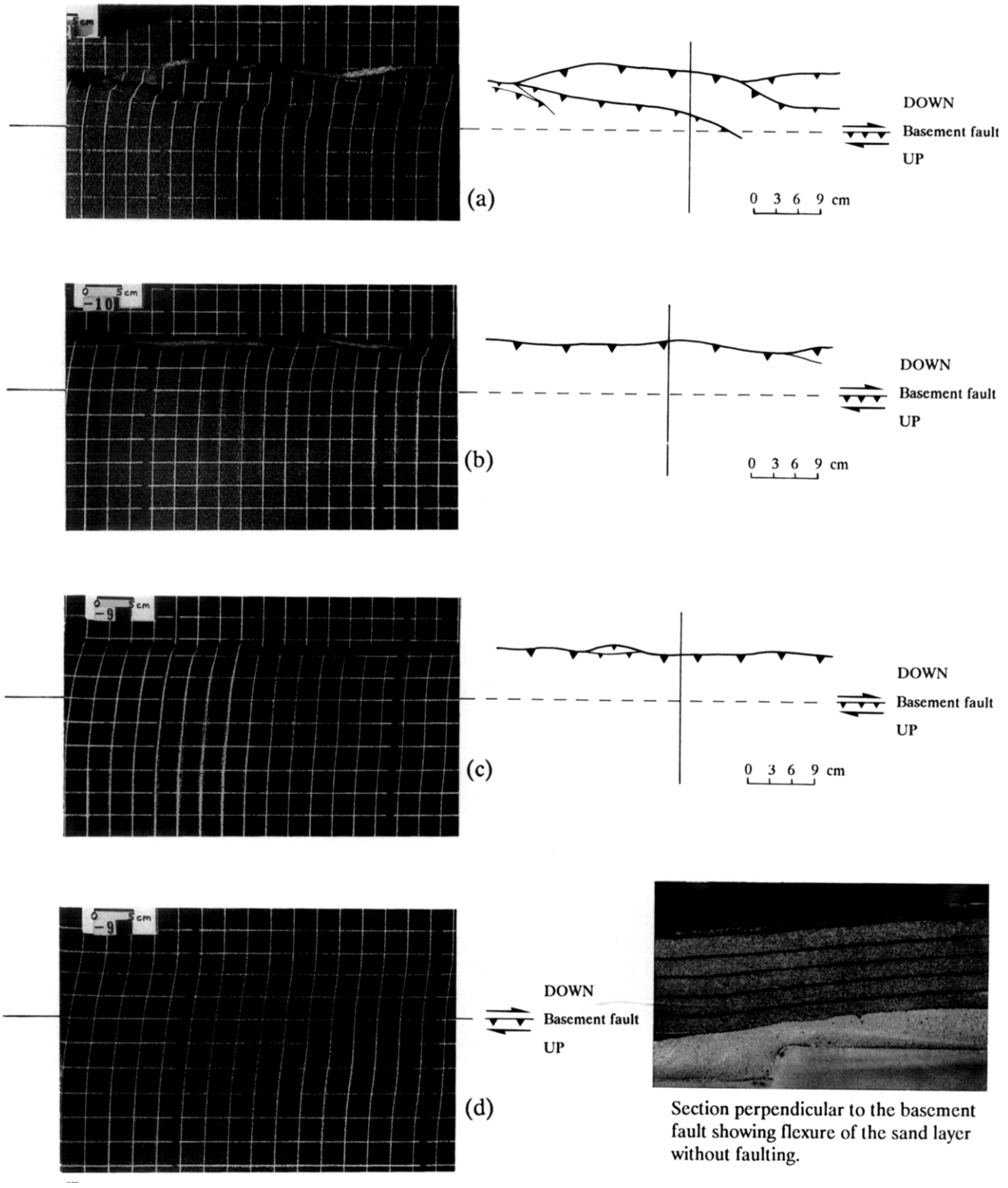

Fig. 5. Reverse oblique-slip experiments ($SS/DS = 1$). Photographs and line drawings of faults developed with the same reverse oblique-slip (4 cm), above a 54° basement fault, with an underlying 0, 1, 2 and 3 cm thick (a–d) layer of silicone. Note the bulk shearing of the overburden in cases (c) and (d).

ment fault was 45° and in reverse oblique-slip experiments, 54°. Thin markers of white sand were deposited on the free surface of each model to serve as material grids for registering displacements and fault motions. Vertical components of fault motion were detected by photographing the free surface under oblique lighting. After faulting, each model was impregnated with water to give cohesion, and cut in a series of vertical cross-sections perpendicular to the basement fault.

EXPERIMENTAL RESULTS

Normal oblique-slip experiments

In surface views of the pure sand model (Fig. 4a), a graben was created parallel and directly above the basement fault. This graben was formed by a normal antithetic fault (in the down-dropped block) and a normal-wrench synthetic fault (in the uplifted block). A

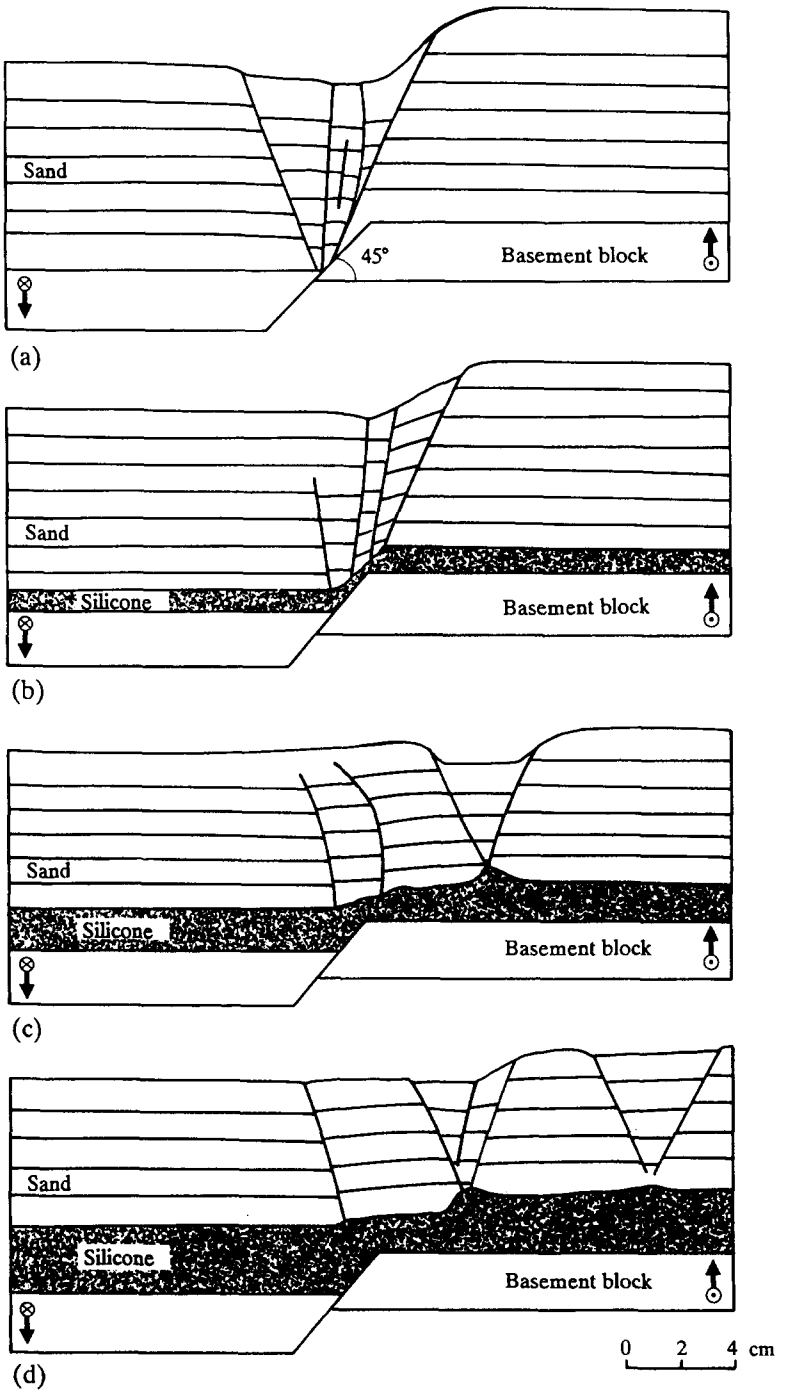

Fig. 6. Normal oblique-slip experiments ($SS/DS = 1$). Line drawings of cross-sections through faulted zone formed above a 45° basement fault, with the same normal oblique-slip (4 cm), with an underlying 0, 1, 2 and 3 cm thick (a–d) layer of silicone. Note the shifted graben in the uplifted compartment in cases (c) and (d).

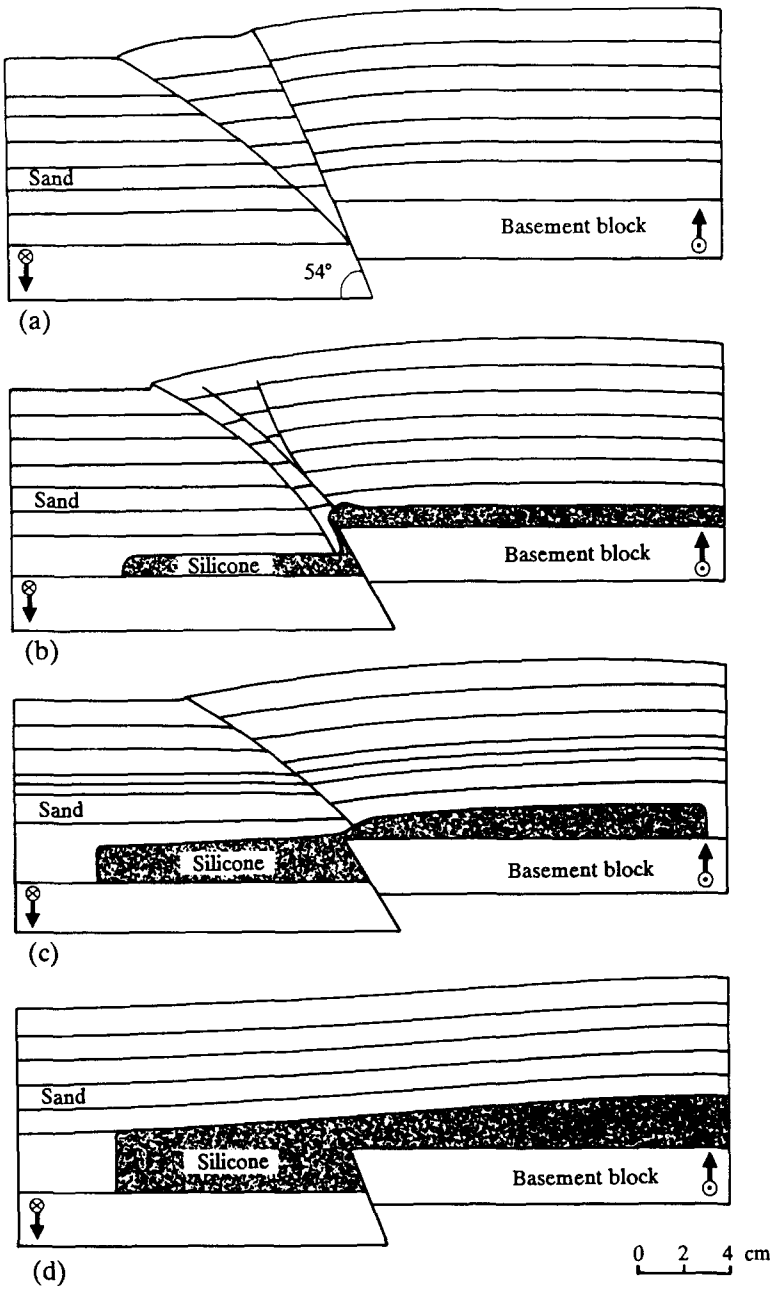

Fig. 7. Reverse oblique-slip experiments ($SS/DS = 1$). Line drawings of cross-sections through faulted zone formed above a 54° basement fault, with the same reverse oblique-slip (4 cm), with an underlying 0, 1, 2 and 3 cm thick (a–d) layer of silicone. Note the absence of faulting with the thickest (3 cm) silicone layer.

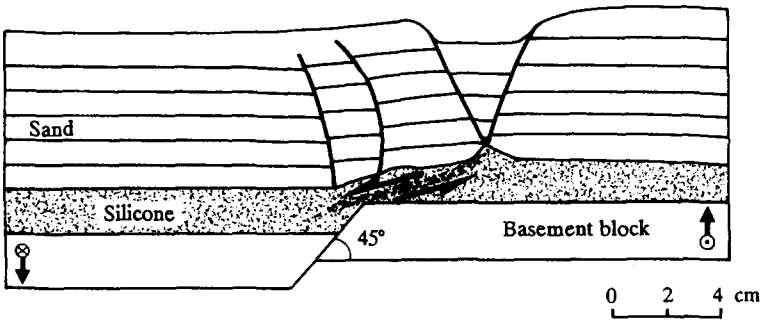

Fig. 8. Interpretation of the flow of the silicone, from the uplifted compartment to the down-dropped compartment, involving the widening of the deformation zone and the creation of a shifted graben in the uplifted compartment.

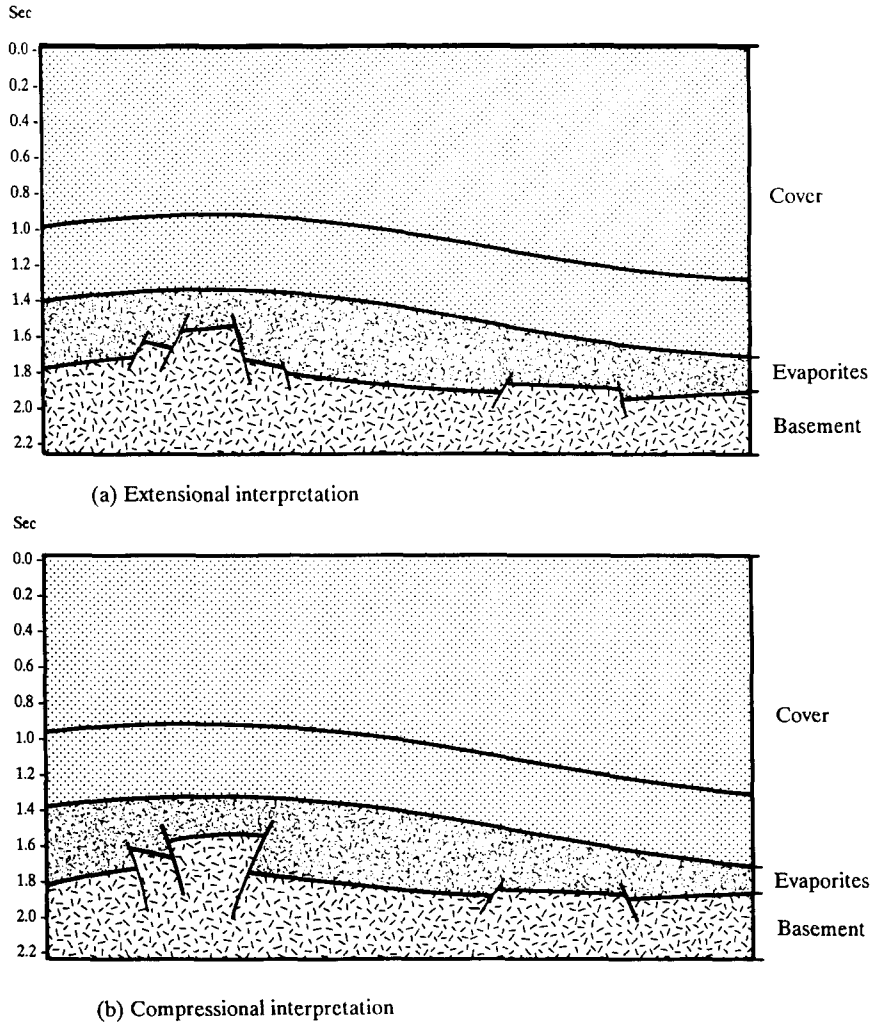

Fig. 9. Alternative interpretation of the same seismic profile. Oblique-slip experiments might favour the compressional interpretation.

strike-slip fault was visible in the middle of the graben. Deformation was strictly limited to the graben.

With a 1 cm thick basal silicone layer (Fig. 4b), no large-displacement antithetic fault was visible. An en échelon pattern of faults appeared directly above the basement fault. This pattern consisted of small-displacement antithetic normal-wrench faults and a large-displacement synthetic normal-wrench fault. Normal oblique-slip motion was seen on each fault. The deformation was limited to the faulted zone.

With a 2 cm thick basal silicone layer (Fig. 4c), deformation was located mostly in the uplifted compartment. Two en échelon small reverse-wrench faults appeared above the basement fault. A large graben, nearly parallel to the basement fault, was created in the uplifted compartment. This graben was formed by two normal-wrench faults, and the outer fault was 7 cm from the basement fault. Many small normal faults were en échelon to the trace of the basement fault, in the uplifted block. Except on the pure normal fault in the lower left corner of the photograph, oblique-slip was observed on the fault planes. The deformation was limited to the faulted zone.

With a 3 cm thick basal silicone layer (Fig. 4d), deformation was located mostly in the uplifted block. Many faults were created en échelon to the trace of the basement fault. One large oblique displacement fault crossed the model, which was reverse-wrench in the left part of the model (close to the basement fault); normal-wrench in the right part (far from the basement fault) and accommodated most of the imposed strike-slip motion. Two grabens were created en échelon to the trace of the basement fault. The outer graben was bounded by two pure normal faults, with no visible lateral offset. The outer fault was 10–12 cm from the basement fault and deformation was limited to the faulted zone.

In cross-sections of the pure sand model (Fig. 6a), a normal antithetic fault with small vertical offset was seen in the down-dropped block. A normal synthetic fault with the large vertical offset was created in the uplifted compartment. The dip of these two faults was about 70°. In the middle of the graben formed by these two faults, were two small vertical offset faults, which were strike-slip. All the faults root in the basement fault.

With a 1 cm thick basal silicone layer (Fig. 6b), most of the faults were synthetic normal faults located in the uplifted compartment. No large antithetic faults were visible in the down-dropped compartment. The faults took root in the sand–silicone interface, on a 3 cm wide

zone. The silicone has been thinned on the border of the uplifted compartment.

With a 2 cm thick basal silicone layer (Fig. 6c), a graben appeared in the uplifted block, far from the basement fault. Two curved reverse faults were created above the basement fault. These faults were en échelon reverse wrench faults, which root in the sand–silicone interface, on a 7 cm wide zone. The silicone has been thickened under the graben and on the border of the down-dropped block and thinned in the uplifted compartment.

With a 3 cm thick basal silicone layer (Fig. 6d), one reverse fault was visible above the basement fault. Two grabens have been created in the uplifted compartment. The silicone has been thickened under the grabens and in the down-dropped compartment and thinned in the uplifted compartment. Faults root in the sand–silicone interface, on a 10 cm wide zone.

Reverse oblique-slip experiments

In surface views, without a silicone layer (Fig. 5a), reverse-wrench faults, slightly en échelon to the trace of the basement fault, characterized the structural pattern in the sand. These faults were located in the down-dropped compartment, and deformation was strictly localized in the faulted zone. With a 1 and 2 cm thick basal silicone layer (Fig. 5b and 5c), one major reverse-wrench fault was created parallel to the basement fault, in the down-dropped compartment. These faults seem to accommodate most of the imposed dip-slip motion and a small part of the imposed strike-slip motion. The marker deformation indicated that most of the strike-slip motion was accommodated by a bulk shearing of the cover, particularly in the hangingwall of the uplifted compartment. With a 3 cm thick basal silicone layer (Fig. 5d), no fault appeared in the overburden, but a bulk shearing of the overburden was visible. Without silicone the deformation zone was 10 cm wide and limited to the faulted zone. With silicone, the deformation zone was no longer limited to the faulted zone, and was 15–17 cm wide with a 1 cm thick silicone layer, 20 cm wide with a 2 cm thick silicone layer, and 24–28 cm wide with a 3 cm thick silicone layer.

In cross-sections of the brittle experiment (Fig. 7a), oblique reverse faults were developed in the down-dropped compartment, which root in the basement fault. The deformation was located in the faulted zone. With 1 and 2 cm of silicone (Figs. 7b & c), the importance of the reverse faults diminished. Faults root in the sand–silicone interface on the uplifted compartment and the deformation zone was no longer limited to the faulted area, but a flexure of the overburden was evident in the uplifted compartment. With a 3 cm thick basal silicone layer (Fig. 7d), no fault appeared in the overburden. The reverse dip-slip component was accommodated in a gentle monocline in the sand layers and by flow in the silicone. The silicone was thinned in the uplifted compartment and thickened in the down-dropped compartment.

CONCLUSION–DISCUSSION

To model deformation during oblique-slip, layered silicone–sand models have been deformed. With a basal silicone layer, the influence of the basement fault on the deformation in the overburden decreased. With no silicone layer, all faults root in the basement fault, but with a basal silicone layer, faults root in the sand–silicone interface over a wide zone. In each experiment with a basal silicone layer, the silicone has been thickened in the down-dropped compartment and thinned in the uplifted compartment. In fact, during the deformation, the silicone flowed (Fig. 8) from the uplifted compartment to the down-dropped compartment. This flow involved a widening of the zone of deformation. Thus, in reverse oblique-slip experiments (convergent wrenching), the overburden deformation changed from localized faults originating at the basement fault to distributed bulk shearing of the cover as a viscous silicone layer was introduced above the basement fault. The thicker the silicone, the larger the bulk shearing. In normal oblique-slip experiments (divergent wrenching), en échelon grabens spread the deformation of the cover into a wide strip, which was nearly parallel to the basement fault, but shifted into the uplifted compartment. The thicker the silicone, the wider the strip in the uplifted compartment. Vertical offsets have significant consequences on structural style, provided there is a basal silicone layer. Deformation then migrates into the uplifted block.

The contrast between the geometries developed in experiments of convergent and divergent wrenching in the presence of a thick viscous horizon is to be noted. Faulting in the cover is absent in the convergent case (Fig. 5a) but present in the divergent case (Fig. 4a). This may help the petroleum geologist to deduce the movement pattern in horizons below an evaporite interval from the structures developed above it. Figure 9 shows alternative interpretations of the same confidential seismic data. The mode of deformation in the basement of Fig. 9(a) is extensional; the mode of deformation of Fig. 9(b) compressional. The gentle warping and the absence of well-developed extensional structures in the horizon above the salt may be interpreted as an indication that shortening rather than extension produced this structure. A comparison with the sand and putty experiments would favour the interpretation of Fig. 9(b).

Discontinuity between basement faulting and faulting in the cover-rocks over an interval deformed by ductile creep can be produced in simple experiments. Faults do not line up across the viscous interval. This is an important conclusion from the experiments. The deformation accommodated above an evaporite interval may well appear to be geometrically independent from the deformation accommodated in the basement below, even when both were caused by the same deformation event.

Acknowledgements—The experiments were carried out at the Koninklijke Shell Exploratie en Produktie Laboratorium, Rijswijk, The Netherlands. The author thanks Shell Internationale Research Maats-

chappij for permission to publish this paper. Special thanks are given to W. T. Horsfield and I. Van der Molen for helping in the realization of this study.

REFERENCES

Byerlee, J. 1978. Friction of rocks. *Pure & Appl. Geophys.* **116**, 615–626.

Cloos, H. 1928. Experimenten zür Inneren tektonik. *Zentbl. Miner. Geol. Paläeont.* **B**, 609–621.

Davy, P. 1986. Modélisation thermo-mécanique de la collision continentale. Unpublished thèse 3ème cycle, Université de Paris Sud.

Horsfield, W. T. 1977. An experimental approach to basement-controlled faulting. *Geol. Mijnb.* **56**, 363–370.

Hubbert, M. K. 1937. Theory of scale models as applied to the study of geologic structures. *Bull. geol. Soc. Am.* **48**, 1459–1520.

Naylor, M. A., Mandl, G. & Sijpesteijn, C. H. K. 1986. Fault geometries in basement induced wrench faulting under different initial stress state. *J. Struct. Geol.* **8**, 737–752.

Odé, H. 1968. Review of mechanical properties of salt relating to salt dome genesis. *Spec. Pap. geol. Soc. Am.* **88**, 544–595.

Ramberg, H. 1967. *Gravity, Deformation, and the Earth's Crust.* Academic Press, New York.

Richard, P. 1990. Champs de failles au dessus d'un décrochement de socle. Modélisation expérimentale. Thèse d'Université, Mem. Doc. C.A.E.S.S. Rennes, No. 34.

Richard, P. & Cobbold, P. R. 1989. Structures en fleur positives et décrochements crustaux: modélisation analogique et interprétation mécanique. *C. r. Acad. Sci., Paris* **308**, II, 553–560.

Richard, P., Mocquet, B. & Cobbold, P. R. In press. Experiments on simultaneous faulting and folding above a basement fault. *Tectonophysics.*

Riedel, W. 1929. Zür Mechanik Geologischer Brucherscheinungen. *Zentbl. Miner. Geol. Paläeont. Abh.* **B**, 354–368.

Van Hoorn, B. 1987. Structural evolution, timing and tectonic style of the Sole Pit inversion. *Tectonophysics* **137**, 239–248.

Vendeville, B. 1987. Champs de failles et tectonique en extension: modélisation expérimentale. Thèse 3ème cycle, Université de Rennes, Mem. Doc. C.A.E.S.S. Rennes, No. 15.

Vendeville, B., Cobbold, P. R., Davy, P., Choukroune, P. & Brun, J.-P. 1986. Physical models of extensional tectonics at various scales. In: *Continental Extensional Tectonics* (edited by Coward, P. P., Dewey, J. F. & Hancock, P. L.). *Spec. Publs geol. Soc. Lond.* **28**, 95–108.

Wilcox, R. E., Harding, T. P. & Seely, D. R. 1973. Basic wrench tectonics. *Bull. Am. Ass. Petrol. Geol.* **57**, 74–96.